AD-A269 715

ARMY RESEARCH LABORATORY

Numerical Simulation of Fluid Dynamics and Combustion for Ram Accelerator Projectile/Obturator Interaction

Michael J. Nusca

ARL-TR-198 September 1993

DTIC
ELECTE
SEP 2 1 1993
S A D

APPROVED FOR PUBLIC RELEASE; DISTRIBUTION IS UNLIMITED.

93 3 20 061

93-21867

NOTICES

Destroy this report when it is no longer needed. DO NOT return it to the originator.

Additional copies of this report may be obtained from the National Technical Information Service, U.S. Department of Commerce, 5285 Port Royal Road, Springfield, VA 22161.

The findings of this report are not to be construed as an official Department of the Army position, unless so designated by other authorized documents.

The use of trade names or manufacturers' names in this report does not constitute indorsement of any commercial product.

REPORT DOCUMENTATION PAGE

Form Approved
OMB No. 0704-0188

Public reporting burden for this collection of information is estimated to average 1 hour per response, including the time for reviewing instructions, searching existing data sources, gathering and maintaining the data needed, and completing and reviewing the collection of information. Send comments regarding this burden estimate or any other aspect of this collection of information, including suggestions for reducing this burden, to Washington Headquarters Services, Directorate for Information Operations and Reports, 1215 Jefferson Davis Highway, Suite 1204, Arlington, VA 22202-4302, and to the Office of Management and Budget, Paperwork Reduction Project(0704-0188), Washington, DC 20503.

1. AGENCY USE ONLY *(Leave blank)*	2. REPORT DATE	3. REPORT TYPE AND DATES COVERED
	September 1993	Final Jan 1992 - Dec 1992

4. TITLE AND SUBTITLE

Numerical Simulation of Fluid Dynamics and Combustion for Ram Accelerator Projectile/Obturator Interaction

5. FUNDING NUMBERS

PR: 1L161102AH43

6. AUTHOR(S)

Michael J. Nusca

7. PERFORMING ORGANIZATION NAME(S) AND ADDRESS(ES)

U.S. Army Research Laboratory
ATTN: AMSRL-WT-PE
Aberdeen Proving Ground, MD 21005-5066

8. PERFORMING ORGANIZATION REPORT NUMBER

9. SPONSORING/MONITORING AGENCY NAMES(S) AND ADDRESS(ES)

US Army Research Laboratory
ATTN: AMSRL-OP-CI-B (Tech Lib)
Aberdeen Proving Ground, MD 21005-5066

10. SPONSORING/MONITORING AGENCY REPORT NUMBER

ARL-TR-198

11. SUPPLEMENTARY NOTES

12a. DISTRIBUTION/AVAILABILITY STATEMENT

Approved for public release; distribution is unlimited.

12b. DISTRIBUTION CODE

13. ABSTRACT *(Maximum 200 words)*

Computational fluid dynamics solutions of the Navier-Stokes equations have been applied to both non-reacting and reacting in-bore flowfields for a ram accelerator projectile launch system. In this system, a projectile is injected at supersonic velocity into a stationary tube filled with a pressurized mixture of hydrocarbon, oxidizer, and inert gases. After ignition, the shock system generated by the projectile can result in sustained combustion around and aft of the projectile. This energy release process, which travels with the projectile, also generates high pressures and imparts thrust to the projectile. Experimental observations indicate that the porous obturator may play a significant role in the initiation of combustion after projectile injection. Numerical simulations have been used to investigate the role of the obturator in both the 38mm and 120mm (bore diameter) systems.

14. SUBJECT TERMS

fluid dynamics, hypervelocity guns, Navier Stokes equations, ramjet engines, supersonic combustion, reacting flows

15. NUMBER OF PAGES

42

16. PRICE CODE

17. SECURITY CLASSIFICATION OF REPORT	18. SECURITY CLASSIFICATION OF THIS PAGE	19. SECURITY CLASSIFICATION OF ABSTRACT	20. LIMITATION OF ABSTRACT
UNCLASSIFIED	UNCLASSIFIED	UNCLASSIFIED	SAR

INTENTIONALLY LEFT BLANK

TABLE OF CONTENTS

Accesion For
NTIS CRA&I ☑
DTIC TAB ☐
Unannounced ☐
Justification .....
By .....
Distribution /
Availability Codes
Dist | Avail and / or Special
A-1

DTIC QUALITY INSPECTED 3

INTENTIONALLY LEFT BLANK

LIST OF FIGURES

LIST OF TABLES

INTENTIONALLY LEFT BLANK

Acknowledgment

Mr. David Kruczynski and Mr. Mahar Kiwan contributed to this work in the areas of experimental and numerical data visualization. In addition, Mr. Kruczynski has supported the numerical simulation aspects of the HIRAM project since its inception.

INTENTIONALLY LEFT BLANK

1. INTRODUCTION

Numerical simulation of the ram accelerator has been an ongoing research project at the U.S. Army Research Laboratory (ARL) since 1990 (Nusca 1990, 1991, 1992). Computational fluid dynamics solutions of the Navier-Stokes equations have been applied to turbulent non-reacting and reacting in-bore flowfields for a ram accelerator projectile launch system. Numerical simulations reveal in-bore flowfield details and provide comparison with measured launch tube wall pressures and projectile thrust as a function of velocity. Numerical simulations are also used to investigate the ARL 120mm (bore diameter) ram accelerator system. These simulations are used as a system design aid and as a means by which geometric and fluid dynamic scaling phenomena are investigated.

For non-reacting flow simulations the Rockwell Science Center USA-PG (Unified Solution Algorithm Perfect Gas) code is used (Chakravarthy 1985,1989). In this code the Navier-Stokes equations are cast in conservation form and converted to algebraic equations using upwind and central finite differences and finite-volume formulations. The equations are solved using a second-order TVD (total variation diminishing) scheme. The code is capable of simulating mixed subsonic/supersonic flowfields.

For finite-rate reacting flow simulations the ARL-RAMCOMB (*RAM*jet *COMB*ustion) code (Nusca, May 1990) has been used. The steady 2D/axisymmetric Navier-Stokes equations are written in stream function-vorticity form and solved using a Gauss-Seidel relaxation scheme. These equations include conservation of chemical species and reacting flow source terms in the energy equation. Both one-step/global and three-step finite-rate reaction mechanisms for fuel (CH_4) and oxidizer (O_2) are considered. In addition, the latest versions of the USA-series codes are being utilized (Ota 1988, Palaniswamy 1989). These codes include both equilibrium (USA-EC) and finite-rate (USA-RG) chemistry which is fully coupled to the gasdynamics and are capable of time-accurate simulations. Comparison of results from the USA-RG and RAMCOMB codes will be reported as well as comparisons between the USA-EC code and finite-rate computations.

Results for the ram accelerator projectile excluding the obturator have been published (Nusca 1990,1991,1992). These numerical simulations used non-reacting or reacting flow codes (in the case of the reacting flow previous efforts used a coupling procedure for the USA-PG and ARL-RAMCOMB codes) to simulate the effects of acceleration on the projectile flowfield. Numerical simulations provided a possible explanation of the thrust/velocity curve as well as data on the fluid dynamic and reacting flow scaling effects. These results are not repeated in the present report and the reader is referred to Nusca (Nov. 1991) for details. It is the purpose of the present report to investigate the projectile/obturator separation

and combustion starting process using non-reacting flow codes (USA-PG) as well as a fully coupled finite-rate chemistry code (USA-RG). Whereas previous simulations have been for steady and quasi-steady flows, the present report focuses on time-accurate predictions of time-dependent flow phenomena.

The ram accelerator projectile geometry used in these studies represents a simplification of the actual configuration used for test firings. The actual projectile includes a set of four bore-riding fins that extend from the point of maximum projectile diameter to the projectile base and span the area between the projectile and the launch tube. Exclusion of these fins permits a 2D/axisymmetric calculation and results in a significant computer time savings over the full 3D numerical simulation. Such 3D simulations have been performed with the present codes.

2. BACKGROUND

The ram accelerator technique was first investigated via experimental test firings at the University of Washington (UW) (Hertzberg 1988, Bruckner 1988/1991, Knowlen 1992) The UW ram accelerator facility uses a light gas gun (e.g. helium driver gas) to accelerate projectiles up to 1300 m/s. The muzzle is connected to a perforated tube and evacuation tank which serve as a dump for the driver gas prior to entrance into the 16m long ram accelerator tube. The accelerator tube, which can be divided into sections separated by diaphragms, is filled with a pressurized fuel/oxidizer mixture and is instrumented at 40 axial locations. Instrumentation consists of pressure transducers, fiber-optic light guides, and magnetic transducers. Thin magnetic sheets are mounted in the nose-body joint and in the base of the projectile (see Figure 1). When the projectile passes electromagnetic transducers on the accelerator tube these magnets induce signals that are used to determine the distance-time history (i.e. velocity) of the projectile. Projectile thrust is derived from the velocity history. The ARL 120mm (bore diameter) facility is described by Kruczynski (1992).

The projectile consists of an axisymmetric cone-boattail body (blunt base) with stabilizing fins to center it along the launch tube axis (see Figure 1). The projectile is shaped like the centerbody of a ramjet engine and is injected into a stationary tube filled with a pressurized gas mixture of hydrocarbon fuel (e.g. CH_4), oxidizer and diluents such as CO_2, N_2, He, and Ar. There is no propellant on board the projectile. The tube resembles the outer cowling of a conventional ramjet engine. When the injection velocity is greater than the sound speed of the gas, a strong oblique shock system develops on the projectile which sustains combustion around the projectile. In this way the energy release process travels along with the projectile. Thrust is generated by the action of high pressure reacting gases on the

rear part of the projectile. Various combustion ignition mechanisms have been investigated including a perforated pusher sabot. The initial gas pressure, fuel/oxidizer composition, and sound speed can be selected to achieve the desired acceleration and projectile velocity at tube exit. Diluents are used to tailor the acoustic speed of the mixture so that the initial Mach number of the projectile exceeds the minimum required ($\simeq 2.8$) to start the diffuser (i.e. projectile/tube clearance at maximum projectile body diameter) and tailors the heat release of combustion to a level that stabilizes the shock system on the projectile body. Excessive diluent results in low projectile acceleration levels, whereas insufficient diluent concentration can cause pre-ignition on the projectile forebody and deceleration. In addition, fuel lean mixtures can result in ignition on the projectile forebody.

The total force on the projectile is composed of the drag force on the forebody and a thrust produced by the high pressure combustion products on the projectile afterbody and base. Normally a net thrust is obtained since the pressure of the combustion products is higher than that of the compressed gases downstream of the nose shock. Gas mixtures with higher heat of reaction yield greater net thrust. Significant combustion must occur only on the afterbody of the projectile in order to maximize thrust since combustion on the conical nose contributes to the drag force. As the combustion moves farther behind the cone-boattail junction on the projectile (throat), smaller fractions of the afterbody surface area are exposed to high pressure gases resulting in reduced thrust.

Several modes of ram accelerator propulsion have been investigated experimentally (Bruckner 1988). The first mode applies to projectile operating velocities below the Chapman-Jouguet (CJ) detonation speed of the propellant mixture (Hertzberg 1988) which typically ranges in Mach number from 2.5 to 4 for hydrocarbon fuels. In this mode, the thrust is provided by the high pressure projectile base pressure resulting from a normal shock system stabilized on the body by theorized thermal choking of the reacting flow at full tube area behind the projectile (see Figure 2). One theoretical model of the thermally choked mode predicts that the normal shock recedes along the body as the projectile velocity increases (Bruckner 1988). If the projectile afterbody were to taper to a point and the flow were inviscid, this normal shock would gradually fall back to the full tube area. A normal shock in a constant area duct, followed by heat addition and thermal choking in steady flow, constitutes a CJ detonation wave. Thus, theory predicts that the thrust goes to zero as the projectile velocity approaches the CJ detonation speed of a particular propellant mixture (Bruckner 1988). For projectile speeds as high as 85% of the CJ detonation speed of the mixture, UW has observed that the thrust as a function of Mach number is indeed accurately predicted by the one-dimensional theoretical model of thermally choked mode (Bruckner 1988). At projectile velocities above 85% of the CJ detonation speed, however, the thrust typically

begins to exceed that predicted by the theoretical model, reaching a minimum at velocities near 95% of the CJ detonation speed of the mixture, and then tends to increase with velocity. This trend coincides with the experimentally observed combustion occurring on the projectile body. Combustion on the surface of the projectile, as opposed to solely in the projectile's wake was proposed by the present author based on numerical simulations (Nusca 1991). Experiments have shown that in this second mode called "transdetonative" (typically Mach number 4 to 6), the projectile can accelerate smoothly at or slightly above the CJ detonation speed of the mixture. For operating at higher Mach numbers, a "superdetonative" mode has been investigated (Bruckner 1988). This mode operates at velocities greater than the CJ detonation speed of the mixture. UW has proposed that this supersonic combustion process involves shock-induced combustion, wherein the mixture is ignited by one of several reflected oblique shock waves on the body. The supersonic heat release raises the gas pressure on the afterbody of the projectile, resulting in thrust as reacted propellant expands back to full tube area.

Typically, beyond the superdetonative mode, measured projectile thrust rapidly decreases perhaps due to extensive combustion on the forebody of the projectile. Each of the propulsion modes described above and observed in experiments at the UW has also been observed in numerical simulations (Nusca 1990,1991,1992).

3. NON-REACTING FLOW SIMULATION

The Reynolds-Averaged Navier-Stokes (RANS) equations for 2D/axisymmetric flow are written in the following conservation form. The dependent variables u, v, and e are mass-averaged.

$$\frac{\partial W}{\partial t} + \frac{\partial F}{\partial x} + \frac{\partial G}{\partial y} + \left(\frac{G}{y} - \frac{H}{y}\right)\alpha = 0 \tag{1}$$

$$W = \begin{pmatrix} \rho \\ \rho u \\ \rho v \\ \rho e \end{pmatrix}, \quad F = \begin{pmatrix} \rho u \\ \rho u^2 - \sigma_{xx} \\ \rho uv - \tau_{xr} \\ \rho ue + \dot{q}_x - \sigma_{xx}u - \tau_{xr}v \end{pmatrix}, \quad G = \begin{pmatrix} \rho v \\ \rho uv - \tau_{xr} \\ \rho v^2 - \sigma_{rr} \\ \rho ve + \dot{q}_r - \tau_{xr}u - \sigma_{rr}v \end{pmatrix},$$

$$H = \begin{pmatrix} 0 \\ 0 \\ -\sigma_+ \\ 0 \end{pmatrix}$$

where $\alpha = 1$ for axisymmetric flow and 0 for two-dimensional flow. Normal stress (σ), shear

stress (τ_{xr}), heat transfer ($\dot{q}$), and internal energy (e) are defined in Nusca (Nov. 1991). The flow medium is assumed to be a perfect gas satisfying the equation of state,

$$p = \rho \Re T \tag{2}$$

The following power law was used to relate molecular viscosity to temperature (Mazor 1985):

$$\frac{\mu}{\mu_o} = \left(\frac{T}{T_o}\right)^n \tag{3}$$

where $\mu_o = 0.1716$ MPa, $T_o = 491.6$ R, and $n = 0.64874$. The laminar and turbulent Prandtl numbers, Pr and Pr_t, were assumed constant with values of 0.72 and 0.9 respectively. The ratio of specific heats, γ, was also assumed constant. The specific heat capacities at constant volume and pressure, c_v and c_p, are related as $\gamma = c_p/c_v$ and $\Re = (\gamma - 1)c_p/\gamma$.

Assuming a time-invariant grid and using the transformation of coordinates implied by $\tau = t, \xi = \xi(x,y), \eta = \eta(x,y)$, Equation 1 can be recast into conservation form where ξ and η are the new independent variables and x_ξ, x_η, y_ξ, and y_η are the four transformation coefficients obtained numerically from the mapping procedure (Chakravarthy 1985).

$$\frac{\partial W}{\partial \tau} + \frac{1}{\text{Area}}\left[(y_\eta F - x_\eta G)_\xi + (-y_\xi F + x_\xi G)_\eta + G/y - H/y\right] = 0 \tag{4}$$

The "Area" in Equation 4 denotes the area of the finite volume cell under consideration at the time of discretization of the equations.

The shock/boundary-layer interference flowfield between projectile and launch tube as well as the projectile wake can include regions of recirculating flow. Modeling of these regions can be critical to the overall flowfield solution quality. However, most existing turbulence models either do not treat such regions or do so in a semi-empirical fashion that is frequently inadequate. To improve the predictive capability of separated flows using RANS codes a new turbulence model has been developed (Goldberg 1986). The model is based on experimental observations of detached flows. The model prescribes turbulence kinetic energy (k) and dissipation (ϵ) analytically within backflows. A formula for the eddy viscosity (μ_t) distribution within backflows is derived and used for the RANS equations when the calculations are done inside separation bubbles. Outside of them, another turbulence model (Baldwin-Lomax, 1978) supplies the values of eddy viscosity. While the Baldwin-Lomax turbulence model is used to detect flow separation and to initiate application of the backflow model, the latter model can relocate the separation point.

4. REACTING FLOW SIMULATIONS

4.1 Chemical Reactions. Systems of chemical reactions are usually complex. A hydrocarbon fuel, for example, may contain hundreds of distinct chemical species. During combustion, numerous short-lived intermediate species are formed in addition to the final products that include H_2O and CO_2. Any increase in computational accuracy by including all intermediate species and reaction steps within the framework of a calculation could be defeated by uncertainties in the thermodynamic, transport, and chemical-kinetic properties of these species. In addition, the computational costs of a given reaction mechanism depend primarily on the number of chemical species included, rather than on the number of reactions (Westbrook 1981). It is possible to make useful predictions of combustion processes by confining attention to a postulated global reaction between hydrocarbon fuel and oxidizer that neglects intermediate steps (Westbrook 1981).

$$\text{Fuel} + \delta O_2 + \text{Diluents} \Rightarrow (1+\delta)(CO_2 + H_2O) + \text{Diluents} \tag{5}$$

where δ is the stoichiometric oxidizer/fuel ratio. Several limitations of a global reaction model should be noted (Rogers 1983). During the ignition delay period, when the complete reaction mechanism will predict the gradual buildup of free radicals with little or no perceptible temperature change, a global model will indicate an immediate exothermic (or endothermic) reaction with resulting temperature increase (or decrease). Secondly, the adiabatic flame temperature predicted by the global model will be higher than for the complete multi-step reaction mechanism. This results from the fact that a global model does not include all the product species actually present in the reaction. If very low pressures are avoided, the discrepancy in flame temperature will not be significant (Rogers 1983). This overestimate of the adiabatic flame temperature increases with larger equivalence ratio (fuel/oxidizer) and is directly related to the amounts of CO and H_2 in the reaction products (Westbrook 1981). In addition, flame speed tends to decrease with increasing pressure for most hydrocarbon-air mixtures; thus, it may not be possible to reproduce both high and low pressure ranges with a single reaction rate expression (Westbrook 1981).

Hydrocarbon reactions are commonly used for ram accelerator testing at the University of Washington (Bruckner 1988) for example,

$$\frac{5}{2}CH_4 + 2O_2 + 6N_2 \tag{6}$$

The fuel equivalence ratio, Φ, is a measure of the amount of fuel available for combustion. When $\Phi = 1$, the proportions of fuel to oxygen are stoichiometric. For Φ values smaller than unity fuel should be completely consumed. For the reaction stated above $\Phi = 2.7$ which is considered slightly outside the range of well understood CH_4/O_2 chemical kinetics

(Anderson 1991). This reaction is one of a general class of hydrocarbon reactions investigated by Westbrook and Dryer (1984),

$$C_aH_bO_c + \frac{1}{2}(a + \frac{b}{2} + c)O_2 \Rightarrow aCO + \frac{b}{2}H_2O \tag{7}$$

where elemental and diluent species N_2, C_2, and H_2 are ignored thus (a=1, b=4, c=1),

$$CH_4 + 2O_2 \Rightarrow CO_2 + 2H_2O \tag{8}$$

CH_4 is considered the fuel, O_2 the oxidizer, and products are CO_2 and H_2O. A three-step reaction mechanism has also been proposed by Westbrook (1991) in which CH_4 is oxidized to CO and H_2 with subsequent oxidation of CO and H_2 forming CO_2 and H_2O.

$$\begin{aligned} CH_4 + 2O_2 &\Rightarrow CO + 2H_2 + \frac{3}{2}O_2 \\ CO + \frac{1}{2}O_2 &\Rightarrow CO_2 \\ 2H_2 + O_2 &\Rightarrow 2H_2O \end{aligned} \tag{9}$$

4.2 Reaction Rates and Kinetics. Conservation of chemical species can be written for each specie in Equations 8 and 9. Because a rate term is included the governing equations are mathematically stiff. Stiffness can be defined as the ratio of the largest to the smallest time scale. In reacting flows, time scales associated with chemistry tend to be much smaller than time scales of the fluid motion, sometimes by orders of magnitude. In the present code the stiffness problem is resolved by uncoupling the fluid dynamics equations from the species conservation (rate) equations for a fixed number of numerical iterations (or sub-iterations between time steps), then updating the rate terms. The reaction rate is defined (Westbrook 1981, 1984) using the Law of Mass Action and an Arrhenius expression for C, the specific reaction rate constant.

$$R = C\prod_{1}^{N} m_j^{n_j} = \bar{A}T^{\alpha}\exp\left(\frac{-E_a}{\bar{\Re}T}\right) m_{CH_4}^{a} m_{O_2}^{b} m_{CO}^{c} m_{H_2}^{d} \tag{10}$$

where and $N = 4$ (for Eq. 8), $\bar{A}T^{\alpha}$ is the collision frequency, the exponential term is the Boltzmann factor, and E_a is the activation energy. The reactant mass fraction terms ($m_{CH_4}^{a}, m_{O_2}^{b}$) for the 1-step reaction mechanism (Eq. 8) are raised to non-stoichiometric coefficients in order to simulate the rate limiting step ($CO+\frac{1}{2}O_2 \Rightarrow CO_2$) of the 3-step mechanism (Eq. 9). For reaction sets given by Equations 8 and 9, Westbrook (1977, 1981, 1984) specifies $\bar{A}$, E_a, a,b,c and d with $\alpha = 0$ and $\bar{\Re} = 8.314$ J/K-mole (see Table 1).

Westbrook and Dryer (1981) used a simple procedure for obtaining the single-step reaction rate expression (Eq. 10). Values for the concentration exponents a and b were held fixed

Table 1. Reaction Rate Equation Data

Reaction	E_a (kcal/mole)	$\bar{A}$ (moles/cm^3-s)	a	b	c	d
Eq. 8	30.0	8.3x10^5	-.3	1.3	0.0	0.0
Eq. 9, step 1	30.0	8.3x10^5	1.0	2.0	0.0	0.0
Eq. 9, step 2	44.7	3.0x10^6	0.0	0.5	1.0	0.0
Eq. 9, step 3	37.6	1.0x10^5	0.0	1.0	0.0	2.0

at the values stated above. They found that the relation $a + b = 1$ was necessary in order to properly reproduce the correct dependence of flame speed on pressure for gas mixtures where Φ is not unity. As expected the flame speed depends strongly on a for fuel-rich mixtures. For $a = -.3$ the fuel acts as an inhibitor which matches observations for methane ignition in shock tubes. The activation energy, E_a, was also held fixed and the pre-exponential factor $\bar{A}$ was varied until the model correctly predicted measured flame speed for atmospheric pressure and $\Phi = 1$. The resulting rate expression was then used to predict flame speed for other values of pressure and Φ. Each set of rate expression parameters was evaluated on the basis of how well it reproduced experimental data (flame speed). The results showed that varying E_a from 26-50 kcal/mole (for Eq. 8) effected the flame thickness alone. Westbrook (1981) suggests $E_a = 30$ and 48.4 kcal/mole as the most appropriate values.

4.3 Governing Equations. The conservation equations for mass (global) and momentum are the same as those given in Equation 1. Additionally, for reacting flows, species mass conservation is given by,

$$\frac{1}{r}\left[\frac{\partial}{\partial r}\left(r\rho u m_j + r J_{j,r}\right) + \frac{\partial}{\partial z}\left(r\rho w m_j + r J_{j,z}\right)\right] - R_j = 0 \tag{11}$$

where R_j is the reaction rate per unit volume for species j. Energy conservation for a compressible reacting, flow is expressed by the same energy equation as used for non-reacting flow (see Eq. 1) if expressed in terms of the total enthalpy ($\tilde{h}$),

$$\nabla \cdot \left[\rho \vec{V} \tilde{h} + \vec{J}_h + \sum_j h_j \vec{J}_j + \vec{J}_k - \left(u\vec{\tau}_r + v\vec{\tau}_\theta + w\vec{\tau}_z\right)\right] = 0 \tag{12}$$

where $\vec{J}$ is a flux term for mass ($\vec{J}_j = (\mu_{\text{eff}}/\text{Re})\nabla m_j$), heat ($\vec{J}_h = (\mu_{\text{eff}}/\text{Pr})c_{p_j}\nabla T$), and turbulence kinetic energy ($\vec{J}_k = (\mu_{\text{eff}}/\text{Pr})\nabla k$). The mass fraction and molar specific enthalpy for species j are m_j and h_j, respectively. Radiation flux is neglected in Equation 12.

In Equation 12 the shear stress ($\vec{\tau}$) includes the Reynolds stress with an effective fluid viscosity expressed as the sum of the molecular and turbulent viscosities, $\mu_{\text{eff}} = \mu + \mu_t$.

A Wilke's mixing law is used to compute the chemically reacting mixture viscosity. The calorically perfect gas assumption can be made when the temperature dependence of c_{p_j} for the reactants and products is not well determined. The specific heat can also be formulated using an explicit temperature dependence obtained from tabulated data (Stull 1971).

$$c_{p_j}/\bar{\Re} = A_1 + A_2 T + A_3 T^2 + A_4 T^3 + A_5 T^4 \tag{13}$$

For N species only $N-1$ specie equations must be solved, since the sum of the mass fractions must equal unity. In effect the global continuity equation is the Nth specie equation since the summation of all specie equations yields the continuity equation. The mixture equation of state for a thermally perfect gas follows from Dalton's Law,

$$p = \rho \bar{\Re} T \sum_j^N \frac{m_j}{\mathcal{M}_j} \tag{14}$$

where $\bar{\Re} = \Re \sum_j \mathcal{M}_j$, $\mathcal{M}_j$ is the molecular weight of species j, and $\Re$ is the specific gas constant. Mixture temperature (T) is obtained from the definition of the stagnation enthalpy,

$$\tilde{h} = T \sum_j^N c_{p_j} m_j + \left[1 - \frac{1}{\mathrm{Pr}}\right] \frac{V^2}{2} + \left[\frac{1}{\mathrm{Sc}} - \frac{1}{\mathrm{Pr}}\right] \frac{\tilde{V}^2}{2} + \left[\frac{1}{\mathrm{Sc}} - \frac{1}{\mathrm{Pr}}\right] \sum_j h_j m_j \tag{15}$$

with $V = (u^2 + v^2 + w^2)^{1/2}$, and $\tilde{V}$ is the magnitude of the turbulent (fluctuating) velocity. The Schmidt number (Sc) is assumed to be unity. The Prandtl number (Pr) is assumed to be nearly unity (.9) which is considered adequate for gaseous flows even with combustion (Bradshaw 1981). Mixture viscosity (μ) is defined using Sutherland's expression (Ames Research Staff 1958) for $T \leq 3400$R and using Equation 3 for higher temperatures.

A two-equation turbulence model has been suggested by Kim and Chung (1989) for reacting flows. This model describes the turbulence viscosity (μ_t) as a function of turbulence kinetic energy (k) and dissipation rate (ϵ) as $\mu_t = \rho C_3 k^2/\epsilon$. A set of partial differential equations is written for k and ϵ.

$$\rho w \frac{\partial k}{\partial z} + \rho u \frac{\partial k}{\partial r} - \frac{1}{r}\left[\frac{\partial}{\partial z}\left(r\mu_k \frac{\partial k}{\partial z}\right) + \frac{\partial}{\partial r}\left(r\mu_k \frac{\partial k}{\partial r}\right)\right] = G - \rho\epsilon \tag{16}$$

$$\rho w \frac{\partial \epsilon}{\partial z} + \rho u \frac{\partial \epsilon}{\partial r} - \frac{1}{r}\left[\frac{\partial}{\partial z}\left(r\mu_\epsilon \frac{\partial \epsilon}{\partial z}\right) + \frac{\partial}{\partial r}\left(r\mu_\epsilon \frac{\partial \epsilon}{\partial r}\right)\right] = B \tag{17}$$

$$B = \frac{C_1 G \epsilon}{k} - \frac{C_2 \rho \epsilon^2}{k} \tag{18}$$

$$\frac{G}{\mu_t} = 2\left(\left(\frac{\partial w}{\partial z}\right)^2 + \left(\frac{\partial u}{\partial r}\right)^2 + \left(\frac{u}{r}\right)^2\right) + \left(\frac{\partial w}{\partial r} + \frac{\partial u}{\partial z}\right)^2 \tag{19}$$

where, $\mu_k = \mu + \mu_t/\lambda_k, \mu_\epsilon = \mu + \mu_t/\lambda_\epsilon, \lambda_k = 1, \lambda_\epsilon = 1.3, C_1 = 1.44, C_2 = 1.92, C_3 = .09$. These equations are solved along with the Navier-Stokes equations. Boundary conditions for k and ϵ are $k = 0, \epsilon = .056\mu(\partial u/\partial y)^2/\rho$ for solid walls and $k = 10^{-6}V_\infty^2, \epsilon = k^{1.5}/L$ for freestream. Initial conditions are $k = k_\infty, \epsilon = k^{1.5}C_3^{-0.5}/(.37x^{0.8}\mathrm{Re}^{-0.4})$.

5. NUMERICAL ALGORITHMS

The spatial discretization technique for the equations of motion must be reliable and robust if it is to successfully capture the complex physics of in-bore projectile/launch tube interacting flowfields. The TVD formulation for the convective terms along with a special treatment of the dissipative terms provides an appropriate simulation. In recent years, TVD formulations have been constructed for shock-capturing finite-difference methods (Chakravarthy 1985). Near large gradients in the solution (extrema) TVD schemes automatically reduce to first-order accurate discretizations locally while away from extrema they can be constructed to be of higher-order accuracy. This local effect restricts the maximum global accuracy possible for TVD schemes to third order for steady-state solutions. TVD methods manifest many properties desirable in numerical solution procedures. By design they avoid numerical oscillations and "expansion shocks" while at the same time being of higher-order accuracy. TVD formulations are also based on the principle of discrete or numerical conservation which is the numerical analog of physical conservation of mass, momentum, and energy. Thus, TVD schemes can "capture" flowfield discontinuities (e.g. shock waves) with high resolution. At a fundamental level they are based on upwind schemes; therefore, they closely simulate the signal propagation properties of hyperbolic equations. Schemes based on the TVD formulation are completely defined. In contrast, schemes based solely on central differences involve global dissipation terms for stability and have one or more coefficients that must be judiciously chosen to achieve desirable results. Any conventional time discretization method suitable for the Navier-Stokes equations can be used together with this space discretization methodology; for example, approximate factorization and relaxation techniques.

5.1 Flowfield Grids. Computing in-bore projectile flowfields is complicated by the multi-wall geometry. The ram accelerator projectile consists of several sharp corners that would severely hamper conventional grid generation schemes that require one set of grid lines to be tangent to surfaces and another set to be normal to them. This geometry is more easily gridded by the zonal approach. The internal geometry of the ram accelerator launch system in broken up into three zones of simple geometric shape (zone 1 between the projectile and the launch tube, zone 2 in the projectile wake and zone 3 aft of the obturator).

An algebraic grid is generated in each zone with clustering near surfaces and other regions in the flowfield where high gradients are expected. The zonal boundaries are transparent to flowfield phenomena (e.g. shock waves). The actual grid used for these computations ($\simeq$ 56,000 nodes) consisted of the following dimensions for zones 1 and 2/3: 261x41, 741x61. The computational domain starts a small distance forward of the body and extends 4.5 projectile body lengths downstream. The computational results were found to be essentially independent of further grid refinement when all other factors were the same. A dense grid is preferred for resolving flow details within boundary layers, to prevent shock smearing, and to resolve shock/boundary-layer interactions.

6. RAM ACCELERATOR CONFIGURATIONS

For the simulation of projectile/obturator separation, the University of Washington 38mm system shot CS10 (N_2 gas fill) was used (Knowlen 1992). The projectile consisted of a 12.5-degree, 65mm long conical forebody and 6.25-degree, 50.8mm long conical afterbody. The projectile base diameter was 17.8mm. The obturator was 14.2mm thick (12 grams) and consisted of 5mm diameter holes, 19 in number or approximately 33% porous. For the reacting flow simulations, the projectile consisted of a 10-degree, 83mm conical forebody and 8-degree, 71mm conical afterbody. The obturator was 16mm thick and consisted of 5mm diameter holes, 19 in number or approximately 33% porous. For comparison to the ARL 120mm ram accelerator system these 38mm system configurations were not simply scaled but the actual 120mm system geometry was used. The projectile consisted of a 10-degree, 261mm conical forebody and 4-degree, 261mm conical afterbody. The obturator was 112mm thick (1.1915 kg) and was assumed to be of the same porosity as the 38mm system. In all configurations the projectile fins were ignored as well as the non-porous obturator backplate.

7. RESULTS

Simulation of the projectile/obturator separation (ignoring the separation of the solid obturator backplate) was accomplished by assuming that the projectile and obturator were mated as they entered the accelerator tube from the launch tube. Simulation of the launch tube section of the system is addressed by Nusca (Oct. 1992). The velocity of the projectile as it traversed the accelerator tube was measured for the University of Washington's shot CS10 and was specified in the simulation. Separation of the obturator due to the aerodynamic forces acting on both sides of the disk was simulated by computing a obturator force coefficient as the time-accurate simulation was run. This coefficient along with the

obturator mass was used to update the obturator position (and re-grid zones 2 and 3 of the computational domain) with respect to the projectile, during the run. The simulation was stopped periodically (corresponding to the location of measurement stations on the University of Washington's system) to examine the accelerator tube wall pressure and compare to measured data. The results included in this report focus on the first two stations (i.e. up to .751m from the entrance) although the simulation was run for 3.0m along the accelerator tube (6m in length). For CS10 the tube was filled with nitrogen gas at 35 atm. The entrance velocity of the projectile/obturator was taken as 1335 m/s (from measurements). The 120mm system used for comparison has a fill pressure of 68 atm and entrance velocity of about 1200 m/s. The numerical simulation was performed from the fixed projectile reference frame with the accelerator tube moving at a fixed (or variable) velocity along with a slug of gas upstream of the projectile. As a result, the boundary layer on the accelerator tube wall does not form until the first shock reflection. The holes in the obturator were treated by assuming uniform porosity of 33%.

Figure 3 shows the projectile velocity versus distance along the accelerator tube as measured at the University of Washington (shot CS10) used for the simulations. The computed obturator velocity, initially the same as the projectile's rapidly decreased as measured but at values about 15% higher. For the 120mm system, the obturator velocity is about 10% lower indicating that it separates more slowly. This is not only due to the mass of the 120mm system obturator but the lower pressures on the obturator surface (relative to those in the 38mm system). Scaling of the fluid dynamics has therefore not been completely accomplished.

Figure 4 shows the computed obturator force coefficient as a function of separation from the projectile. Initially the force is high, but as the obturator separates from the projectile this force decreases (relief effect) and then increases with separation distance. The shielding of the obturator from the oncoming flow (relative to the projectile-based coordinate system) is gradually removed and the drag rises. The force on the obturator for the 120mm system, for the same relative separation distance, is slightly smaller initially and slightly greater at larger separation. This indicates a lower initial obturator surface pressure, as mentioned previously.

Figures 5 illustrates the flowfields over the projectile/obturator configurations at measurement stations 1 and 2 (as well as pre-station 1) in the 38mm system. These pressure contours highlight areas of large pressure gradients and show that the projectile base flow is effected by the presence of the obturator.

Figures 6 and 7 show the accelerator tube wall pressure as measured in the University of Washington's 38mm system and computed in the ARL simulation. Figure 6 shows station 1

(just after entrance to the accelerator tube) pressures where the obturator is computed to be located approximately 78mm (67% projectile length) behind the projectile base (note that the projectile is .116m long). Pressure rises over the projectile are indicative of nose-shock reflections from the tube wall. These pressures are smaller than measured due to the absence of the projectile fins in the simulation. The double pressure peaks in front of the obturator location are seen in the measured and computed data. As indicated previously the obturator is slightly aft of the measured location (higher velocity, see Figure 3) in the simulation. The smaller pressure computed behind the obturator location is due to the downstream boundary condition imposed (i.e. tube fill pressure as opposed to gas pressure with venting created by the launch/vent tube which was not part of the present simulation). Figure 7 shows results for station 2 where the obturator is computed to be approximately 240mm (200% projectile length). The overall pressure levels are lower and the agreement between measured and computed data is better. The measured pressure rise at about .25m in Figure 7 occurs at about .28m in the simulation. The back pressure mismatch is again due to the downstream pressure boundary condition.

Figures 8 and 9 compare the computed accelerator tube wall pressures for the 38mm and 120mm systems. Due to the different projectile lengths, the x-axis has been made nondimensional. The gas pressure in the 38mm system was 35 atm while the 120mm system was charged to 68 atm. Since the 120mm system projectile has a different forebody angle (see section "Ram Accelerator Configurations") the pressure spikes are larger and at slightly different locations for this system. The pressures in the vicinity of the obturator are slightly lower for the 120mm system at station 1 (Figure 8) but slightly higher at station 2 (Figure 9), which is consistent with the data in Figure 4. As the obturator separates more significantly from the projectile (Figure 9) trends in pressure levels (downstream of the projectile) are comparable for the two systems. This reflects the fact that some fluid dynamic analysis has been used in the design of the 120mm system projectile in order to achieve a good scaling match to the 38mm system.

Figure 10 shows the results from a projectile/obturator separation simulation for reacting flow, methane/oxygen/nitrogen mixture at 12 atm fill pressure in the 38mm system. The projectile/obturator geometry is slightly different (as detailed in the last section). In this figure the obturator is computed to be approximately 56mm (37% projectile length of 154mm) behind the projectile base. The computation is for finite-rate chemical kinetics (three-step global model). Computed pressures before the reaction zone (before about .12m in the figure) compare well with measured data. In the reaction zone pressures are slightly smaller (due to the simplified chemical kinetics model) for the computation. Pressures near the obturator location are similar to measurements with smaller back pressure since the launch

tube section has been ignored (see previous discussion). Figure 11 shows the projectile thrust in the 38mm system as a function of velocity. Overprediction of the thrust is expected to be corrected when more detailed chemistry models (i.e. more reaction steps) are included.

8. CONCLUSIONS AND FUTURE WORK

Computational fluid dynamics solutions of the Navier-Stokes equations have been applied to both non-reacting and reacting in-bore flowfields for a ram accelerator projectile launch system. Good comparison between computed and measured pressures for non-reacting flow in a 38mm system was achieved, including the investigation of geometric scaling to a 120mm system. Previous publications by the ARL have focused on the simulation of projectile flow phenomena in the accelerator. The present work represents numerical simulation of projectile/obturator separation and the starting mechanism after projectile/obturator entrance into the accelerator tube. Good agreement with measured pressures during obturator separation has been achieved. Application of more detailed reaction kinetic models, as well as the investigation of the launch/vent tube (pre-accelerator) sequence, is warranted.

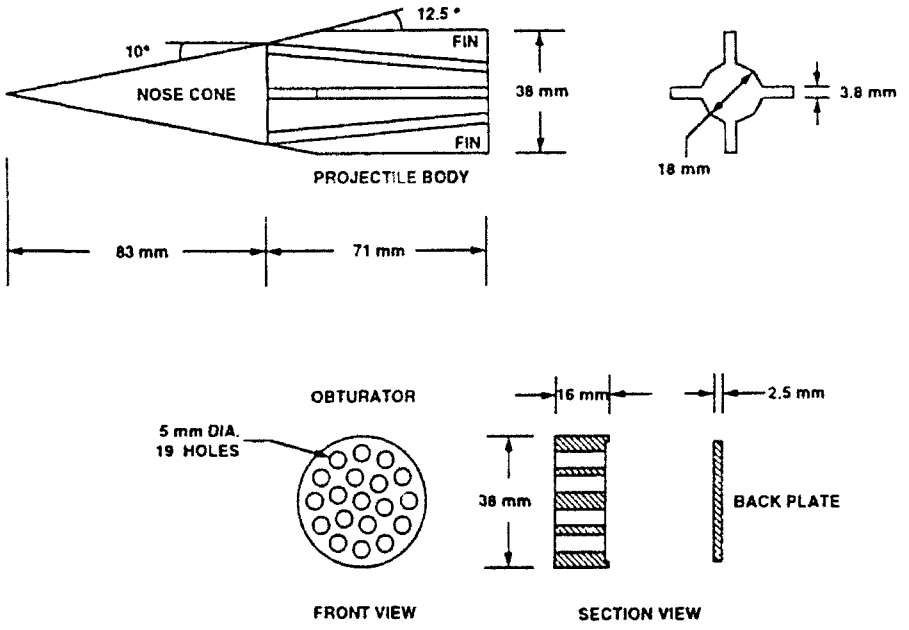

Figure 1. Schematic of projectile and obturator used in University of Washington experiments.

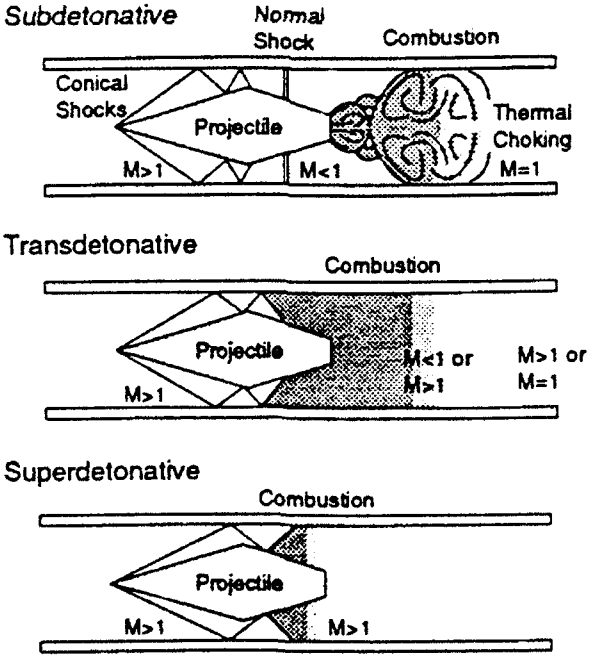

Figure 2. Schematics of thermally choked, transdetonative and superdetonative ram accelerator operating modes.

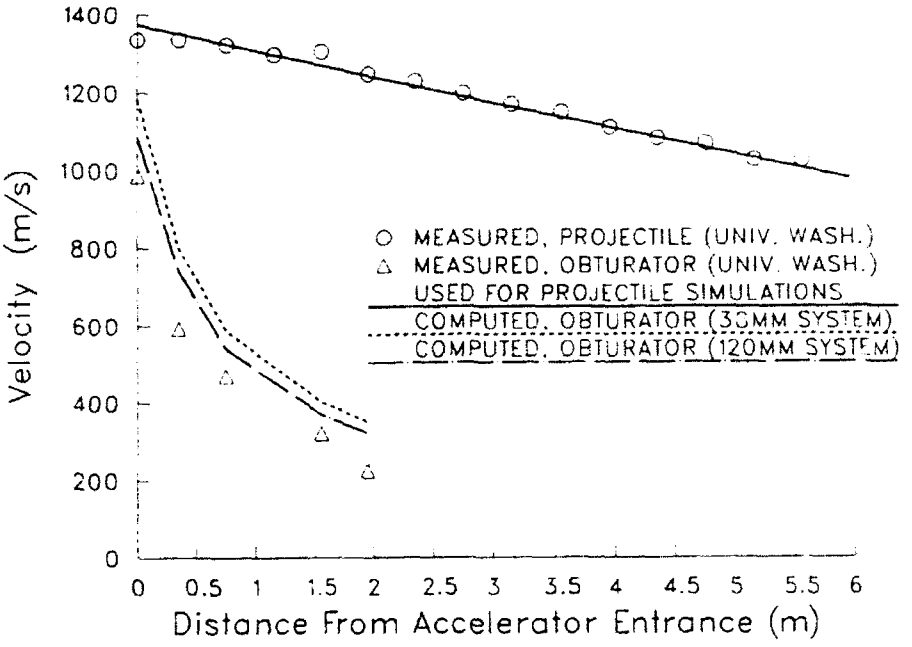

Figure 3. Projectile and obturator velocity along the accelerator tube, nitrogen gas fill (35 atm), 38mm and 120mm systems.

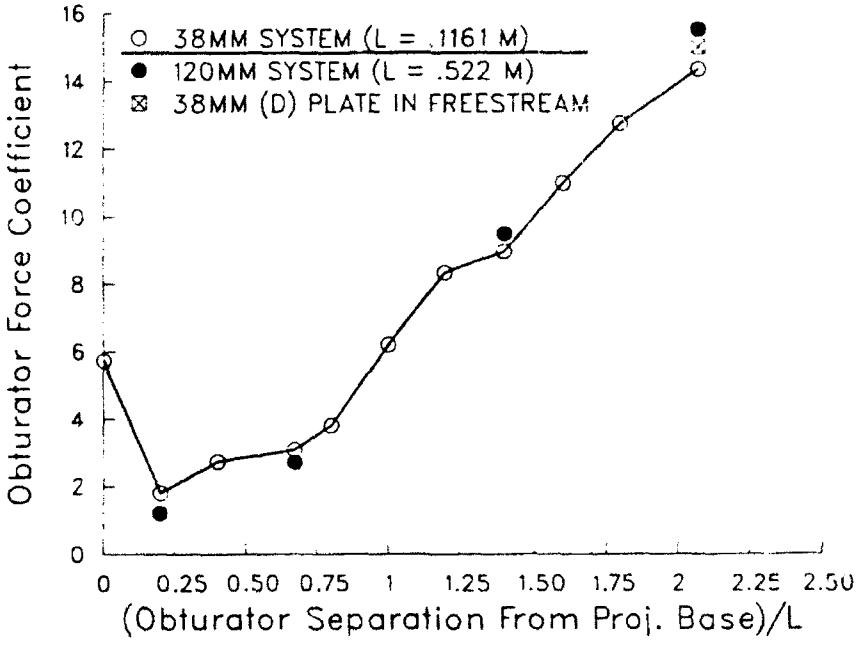

Figure 4. Computed obturator force coefficient (F/PA) as obturator separates from projectile, nitrogen gas fill, 38mm (35 atm) and 120mm (68 atm) systems.

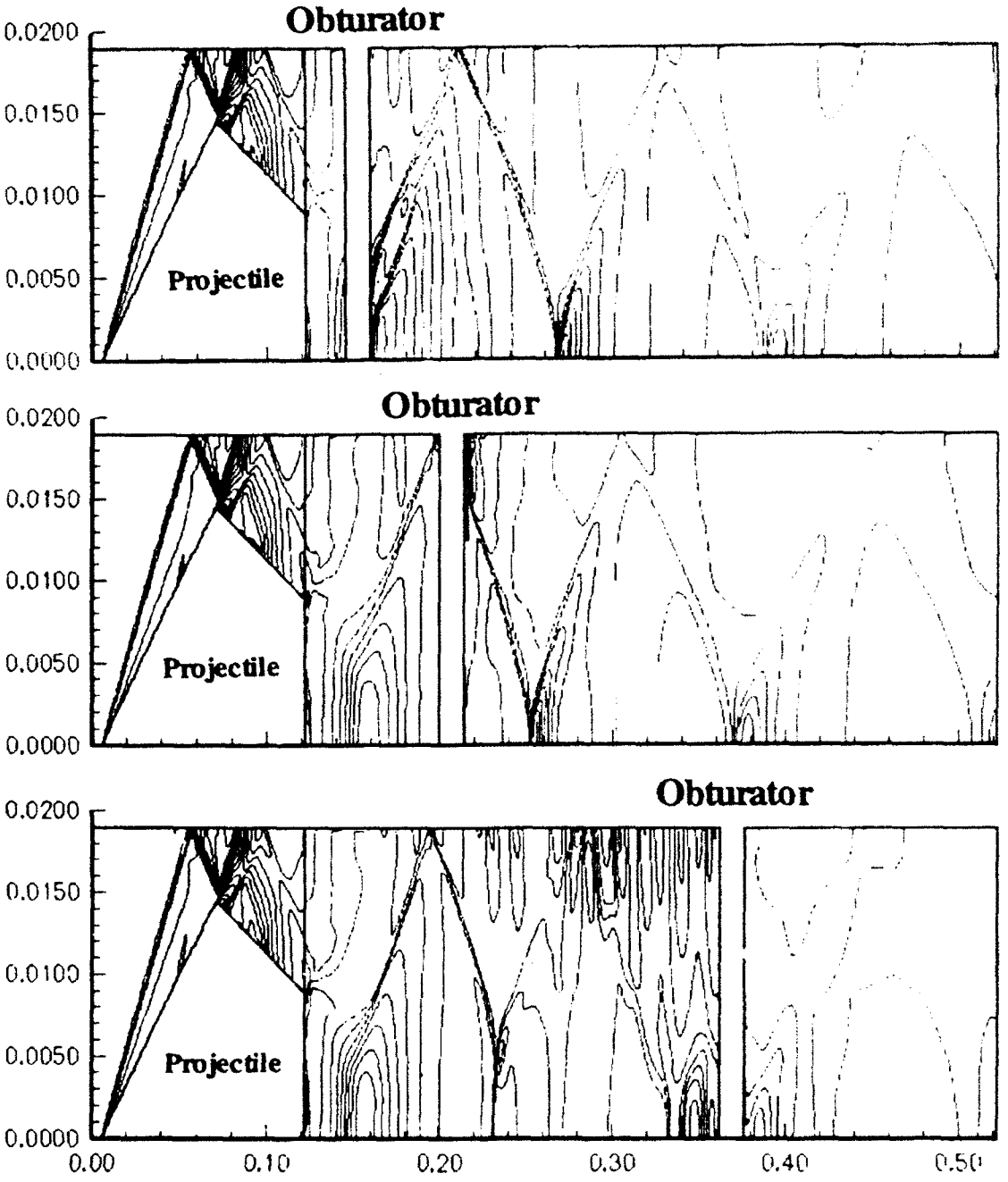

Figure 5. Computed pressure contours for nitrogen gas fill (35 atm), 38mm system, three stations in accelerator tube. Pre-first station with obturator at approx. 0.14 meters (computed), first station with obturator at approx. 0.2 meters (computed),second station with obturator at approx. 0.36 meters (computed). Axes are lengths in meters. Note magnified y-scale, i.e. angles on projectile are not true.

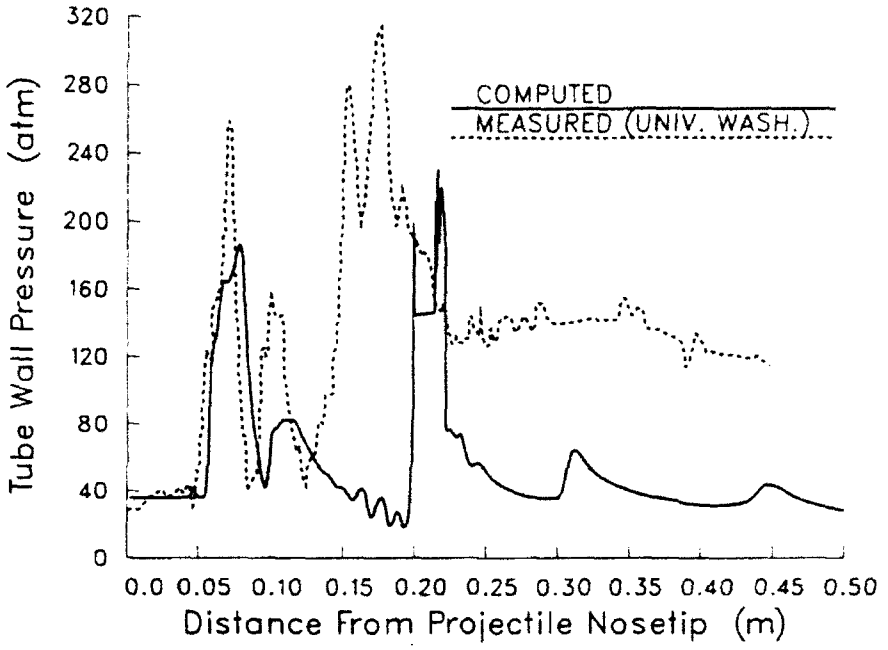

Figure 6. Tube wall pressure for nitrogen gas fill (35 atm), 38mm system, first station in accelerator tube, obturator at approx. 0.2 meters (computed).

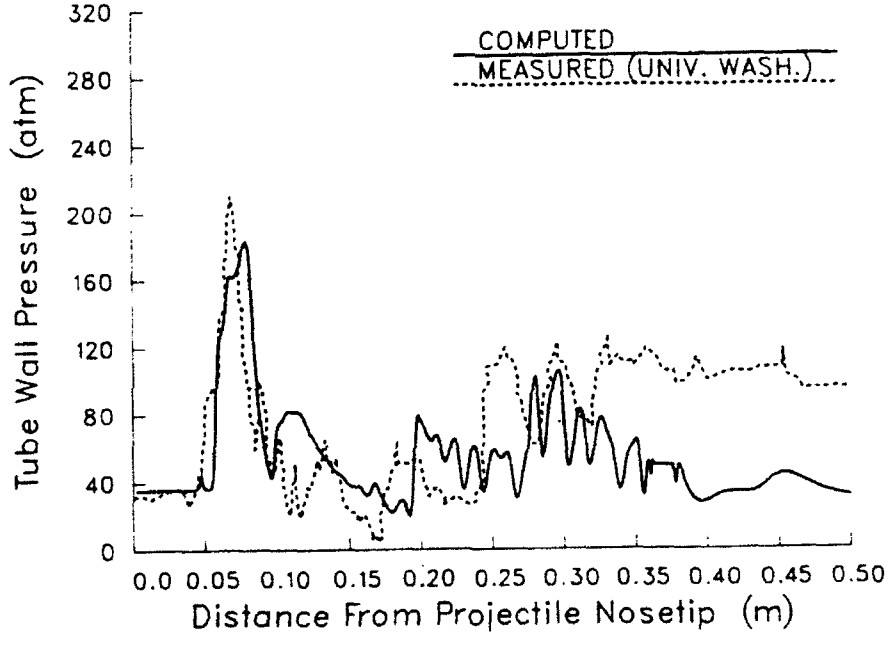

Figure 7. Tube wall pressure for nitrogen gas fill (35 atm), 38mm system, second station in accelerator tube, obturator at approx. 0.36 meters (computed).

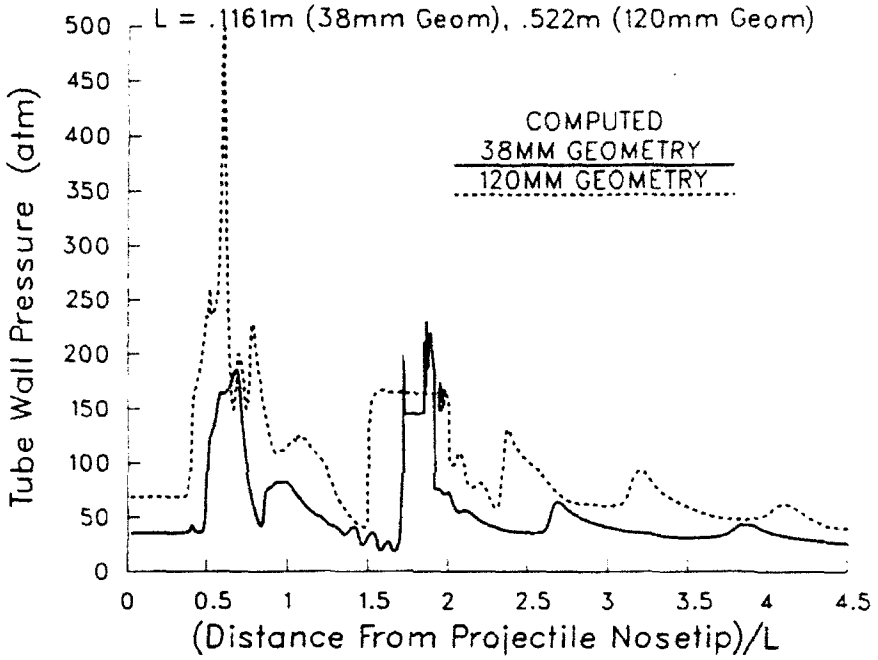

Figure 8. Computed tube wall pressure for nitrogen gas fill, 38mm (35 atm) and 120mm (68 atm) systems, first station in accelerator tube, obturator at approx. 1.7 L (computed).

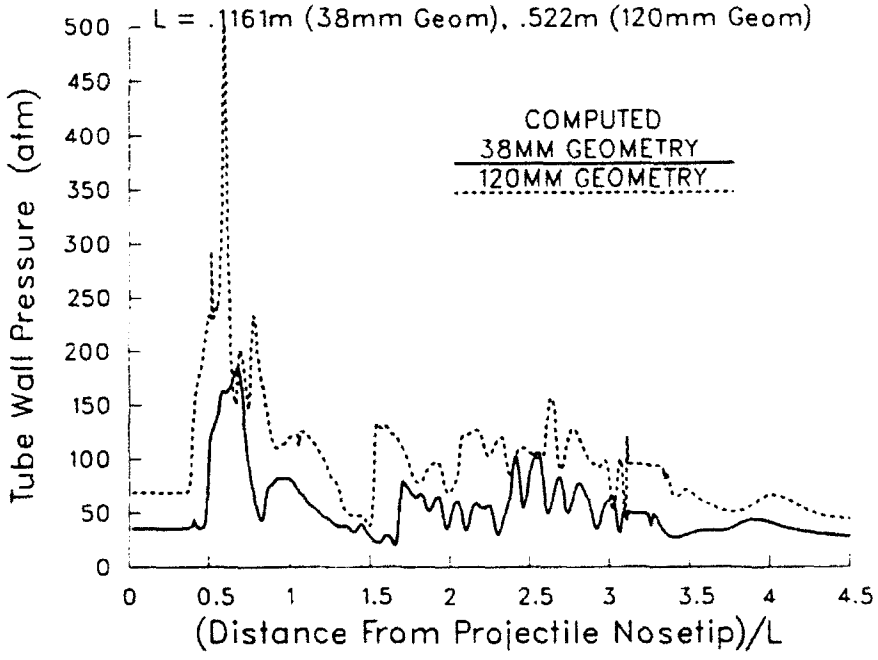

Figure 9. Computed tube wall pressure for nitrogen gas fill, 38mm (35 atm) and 120mm (68 atm)systems, second station in accelerator tube, obturator at approx. 3.1 L (computed).

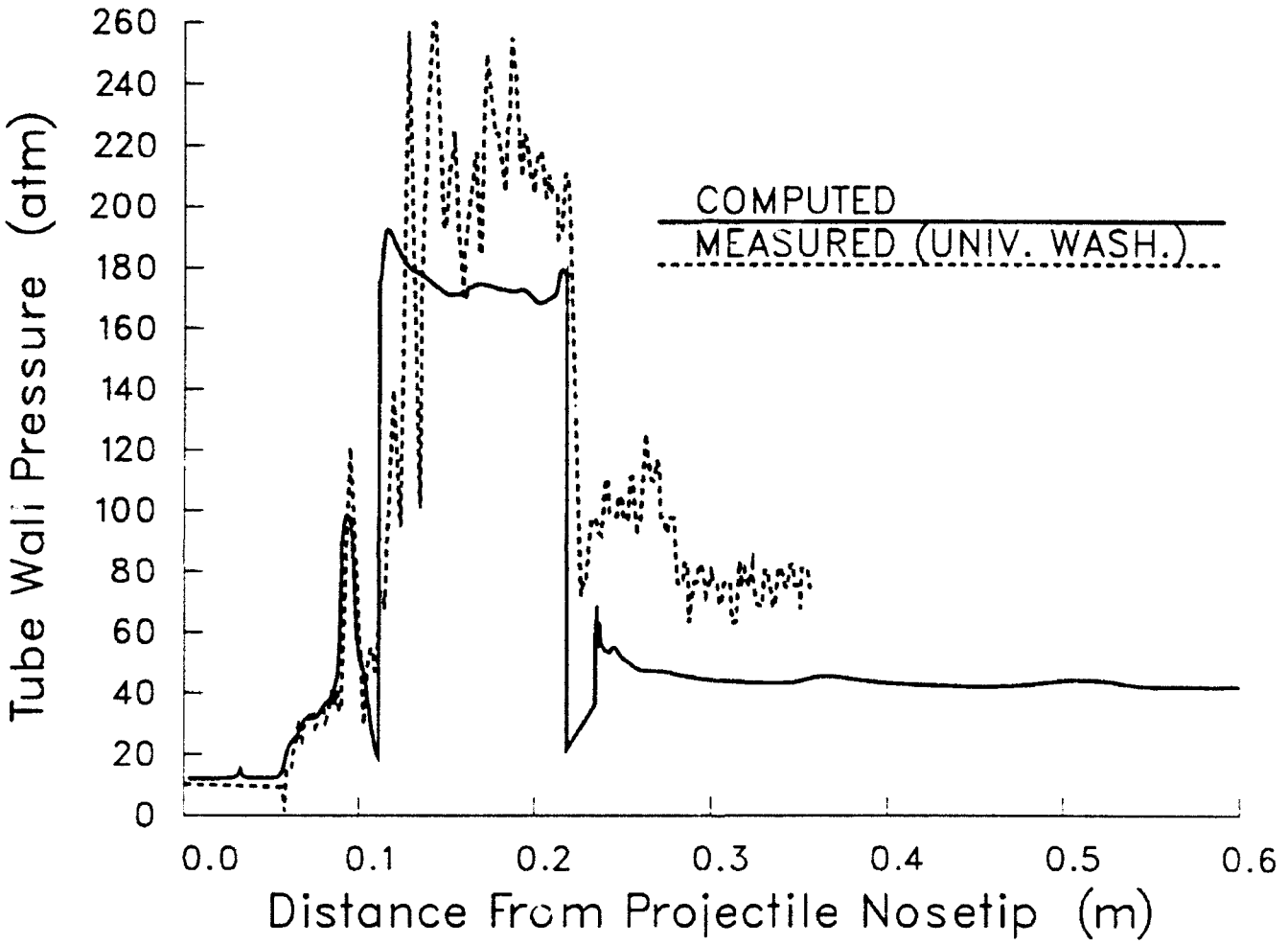

Figure 10. Tube wall pressure for reacting $2.7CH_4+2O_2+ 5.6N_2$ gas fill (12 atm), 38mm systems, first station in accelerator tube, obturator at approx. 0.22 m (measured).

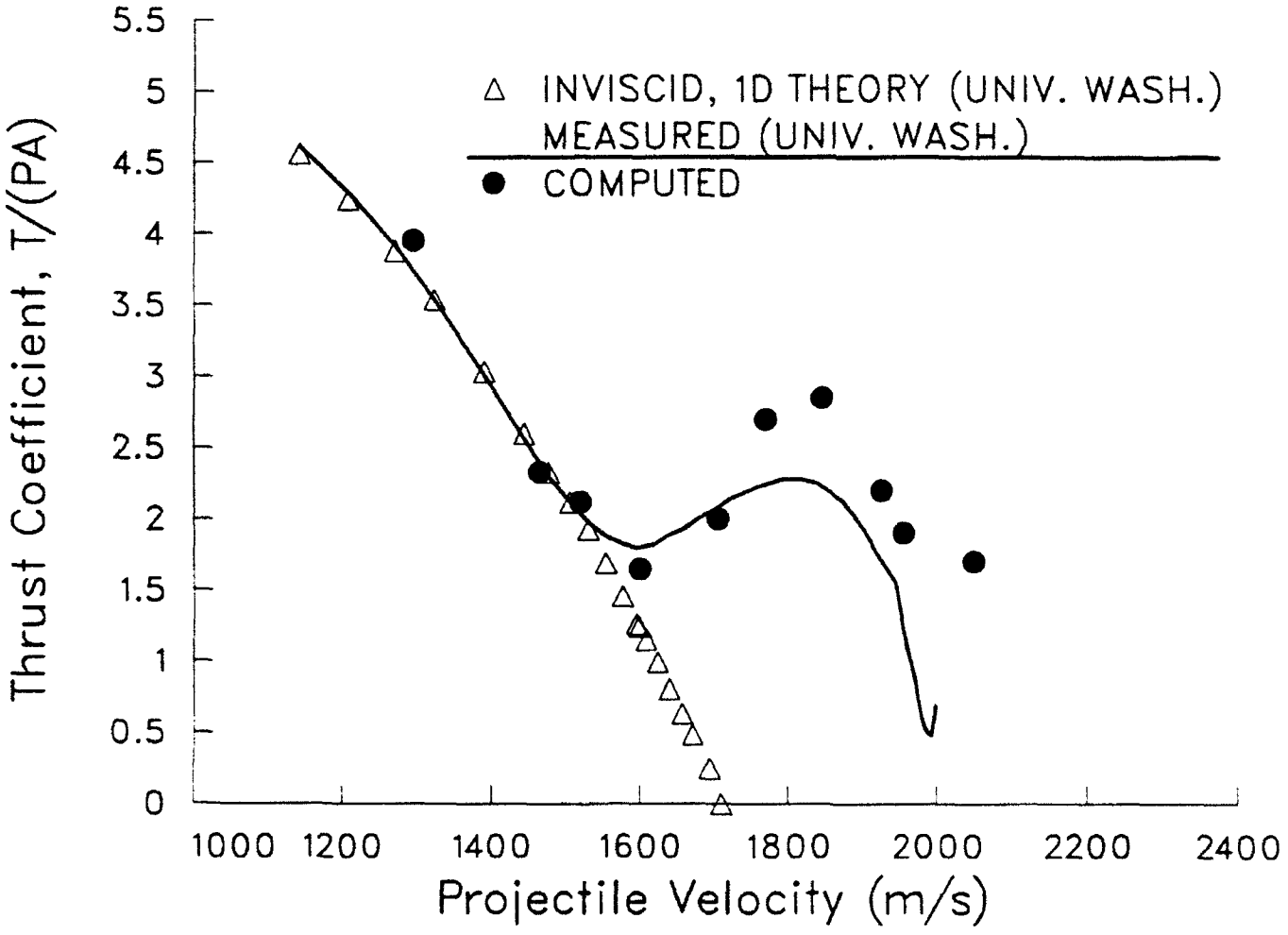

Figure 11. Projectile thrust coefficient vs. projectile velocity for reacting $2.7CH_4+2O_2+5.6N_2$ gas fill (20 atm), 38mm system (A = .0011m ^{2}).

INTENTIONALLY LEFT BLANK

9. REFERENCES

Anderson, W.R., and Kotlar, A.J., "Detailed Modeling of CH_4/O_2 Combustion for Hybrid In-Bore Ram Propulsion (HIRAM) Application," 28th JANNAF Combustion Meeting, Brooks Air Force Base, San Antonio, Texas, Oct. 28 - Nov. 1, 1991.

Ames Research Staff, "Equations, Tables, and Charts for Compressible Flow," NACA Report 1135, 1958.

Baldwin, B.S. and Lomax, H., "Thin Layer Approximation and Algebraic Model for Separated Turbulent Flows," AIAA-78-257, Proceedings of the 16th AIAA Aerospace Sciences Meeting, Huntsville, AL, January 16-18, 1978.

Bradshaw, P., Cebeci, T., and Whitelaw, J.H., Engineering Calculation Methods for Turbulent Flows, Academic Press, New York, 1981.

Bruckner, A.P., Knowlen, C., Scott, K.A., and Hertzberg, A., "High Velocity Modes of the Thermally Choked Ram Accelerator," AIAA-88-2925, Proceedings for the 24th AIAA Joint Propulsion Conference July 11-13, 1988, Boston, MA.

Bruckner, A. P., Burnham, E.A., Knowlen C.,and Hertzberg A. "Initiation of Combustion in the Thermally Choked Ram Accelerator," Proceedings of the 18th International Symposium on Shock Waves, Sendai, Japan, July 21-26, 1991.

Chakravarthy, S.R., Szema, K.Y., Goldberg, U.C., Gorski, J.J., and Osher, S., "Application of a New Class of High Accuracy TVD Schemes to the Navier-Stokes Equations," AIAA-85-0165, Proceedings of the AIAA 23rd Aerospace Sciences Meeting, Jan. 14-17, 1985, Reno, NV.

Chakravarthy, S.R., Szema, K.Y., and Haney, J.W., "Unified Nose-to-Tail Computational Method for Hypersonic Vehicle Applications," AIAA-89-2564, Proceedings of the AIAA 6th Applied Aerodynamics Conference, June 6-8, 1989, Williamsburg, VA.

Goldberg U.C., "Separated Flow Treatment with a New Turbulence Model," AIAA Journal, Vol. 24, No. 10, October 1986, pp. 1711-1713.

Hertzberg, A., Bruckner, A. P., and Bogdanoff, D. W., "Ram Accelerator: A New Chemical Method for Accelerating Projectiles to Ultrahigh Velocities," AIAA Journal, vol. 26, pp. 195-203, 1988.

Kim, Y.M., and Chung, T.J., "Finite-Element Analysis of Turbulent Diffusion Flames," AIAA Journal, Vol. 27, No. 3, March 1989, pp. 330-339.

Knowlen, C., private communication, University of Washington, May 1992.

Knowlen, C., Bruckner, A. P., and Hertzberg A. "Internal Ballistics of the Ram Accelerator," Proceedings of the 13th International Symposium on Ballistics, Stockholm, Sweden, 1-3 June 1992.

Kruczynski, D.L., and Nusca, M.J., "Experimental and Computational Investigation of Scaling Phenomena in a Large Scale Ram Accelerator," AIAA-92-3245, Proceedings of the 28th AIAA Joint Propulsion Conference, Nashville, TN, July 6-8, 1992.

Mazor G., Ben-Dor G., and Igra O., "A Simple and Accurate Expression for the Viscosity of Nonpolar Diatomic Gases up to 10,000 K," AIAA Journal, Vol. 23, No. 4, April 1985, pp. 636-638.

Nusca, M.J., "Steady Flow Combustion Model for Solid-Fuel Ramjet Projectiles," AIAA Journal of Propulsion and Power, Vol. 6, No. 3, May-June 1990, pp. 348-352.

Nusca, M.J., "Numerical Simulation of Reacting Flow in a Thermally Choked Ram Accelerator," Proceedings of the 27th JANNAF Combustion Meeting Warren AFB, Cheyenne, Wyoming, 5-9 Nov. 1990. See also, BRL-TR-3222, U.S. Army Ballistic Research Laboratory, Aberdeen Proving Ground, MD, April, 1991.

Nusca, M. J., "Numerical Simulation of Reacting Flow in a Thermally Choked Ram Accelerator Projectile Launch System", AIAA-91-2490, Proceedings of the 27th AIAA Joint

Propulsion Conference, Sacramento, CA, June 24-26, 1991, AIAA paper 91-2490.

Nusca, M. J., "Navier-Stokes Simulation of Fluid Dynamic and Combustion Phenomena in the RAM Accelerator", Proceedings of the 28th JANNAF Combustion Meeting" Brooks Air Force Base, San Antonio, Texas, Oct. 28 - Nov. 1, 1991.

Nusca, M.J., "Numerical Simulation of Transient Fluid Dynamics and Initiation of Combustion in the Ram Accelerator," Proceedings of the 29th JANNAF Combustion Subcommittee Meeting, NASA Langley Research Center, Hampton, VA 19-22 Oct. 1992.

Ota, D.K., Chakravarthy S.R., and Darling, J.C., "An Equilibrium Navier-Stokes Code for Hypersonic Flows," AIAA-88-0419, Proceedings of the 26th AIAA Aerospace Sciences Meeting, Jan. 11-14, 1988, Reno, NV.

Palaniswamy, S., and Chakravarthy, S.R., "Finite Rate Chemistry for USA Series Codes: Formulation and Applications," AIAA-89-0200, Proceedings of the 27th AIAA Aerospace Sciences Meeting, Jan. 9-12, 1989, Reno, NV.

Rogers, R.C., and Chinitz, W., "Using a Global Hydrogen-Air Combustion Model in Turbulent Reacting Flow Calculations," AIAA Journal, Vol. 21, No. 4, April 1983, pp. 586-592.

Stull, D.R., and Prophet, H., "JANNAF Thermochemical Tables," 2nd ed., National Bureau of Standards, NSRDS-Rept. 37, June 1971.

Westbrook, C.K., Creighton, J., and Lund, C., "A Numerical Model of Chemical Kinetics of Combustion in a Turbulent Reactor," Journal of Physical Chemistry, Vol. 81, No. 25, 1977, pp. 2542-2554.

Westbrook, C.K., and Dryer, F.L., "Simplified Reaction Mechanisms for the Oxidation of Hydrocarbon Fuels in Flames," Combustion Science and Technology, Vol. 27, 1981, pp. 31-43.

Westbrook, C.K., and Dryer, F.L., "Chemical Kinetic Modeling of Hydrocarbon Combustion," Progress in Energy Combustion Science, Vol. 10, 1984, pp. 1-57.

Westbrook, C., private communication, Lawrence Livermore Laboratory, Livermore, CA, June 1991.

LIST OF SYMBOLS

A	cross sectional area of launch tube
c_p	specific heat capacity, constant p
c_v	specific heat capacity, constant volume
C	specific reaction rate constant
e	specific total internal energy
E_a	activation energy
F, G, H	flux vectors (Eq. 1)
h	molar specific enthalpy
$\tilde{h}$	total enthalpy
J	flow rate or flux
k	turbulence kinetic energy
L	total body length
m	species mass fraction
$\mathcal{M}$	molecular weight
n	stoichiometric coefficient
N	number of species
p	static pressure
Pr	Prandtl Number, $\mu c_p/\kappa$
$\dot{q}$	heat transfer rate
r	radial direction
R	reaction rate per unit volume
$\Re$	specific gas constant, $(\gamma - 1)c_p/\gamma$
$\hat{\Re}$	universal gas constant, $\Re \sum_j \mathcal{M}_j$
Re	Reynolds Number, $\rho V L/\mu$
Sc	Schmidt Number, μ/Γ
t	time
T	static temperature
$\mathcal{T}$	thrust

u	axial velocity
v	radial velocity
V	magnitude of the local velocity vector
W	dependent variable vector (Eq. 1)
x, y	cartesian coordinates

Greek Symbols

α	parameter (Eq. 1, 10)
γ	ratio of specific heats, c_p/c_v
Γ	diffusion coefficient
δ	stoichiometric oxidizer/fuel mass ratio
ϵ	turbulence dissipation rate
η	transformed coordinate
κ	heat transfer coefficient
μ	molecular viscosity
ξ	transformed coordinate
ρ	density
σ	normal stress
τ	transformed time
τ_{xr}	shear stress tensor
$\vec{\tau}$	shear stress vector
Φ	fuel equivalence ratio

Superscripts

$\hat{}$	unit vector
$\tilde{}$	total or stagnation
$\dot{}$	rate

Subscripts

eff	effective
h	enthalpy
j	j-th mixture component or species
k	turbulence kinetic energy
p	constant pressure
r	radial component or radial direction
t	turbulence quantity
v	constant volume
x	x-direction
z	axial component
ϵ	turbulence dissipation rate
η	η-direction transform coefficient
θ	azimuthal component
ξ	ξ-direction transform coefficient
∞	freestream quantity

INTENTIONALLY LEFT BLANK

No. of Copies	Organization
2	Administrator Defense Technical Info Center ATTN: DTIC-DDA Cameron Station Alexandria, VA 22304-6145
1	Commander U.S. Army Materiel Command ATTN: AMCAM 5001 Eisenhower Ave. Alexandria, VA 22333-0001
1	Director U.S. Army Research Laboratory ATTN: AMSRL-OP-CI AD, Tech Publishing 2800 Powder Mill Rd. Adelphi, MD 20783-1145
1	Director U.S. Army Research Laboratory ATTN: AMSRL-OP-CI-AD, Records Management 2800 Powder Mill Rd. Adelphi, MD 20783-1145
2	Commander U.S. Army Armament Research, Development, and Engineering Center ATTN: SMCAR-IMI-I Picatinny Arsenal, NJ 07806-5000
2	Commander U.S. Army Armament Research, Development, and Engineering Center ATTN: SMCAR-TDC Picatinny Arsenal, NJ 07806-5000
1	Director Benet Weapons Laboratory U.S. Army Armament Research, Development, and Engineering Center ATTN: SMCAR-CCB-TL Watervliet, NY 12189-4050
1	Director U.S. Army Advanced Systems Research and Analysis Office (ATCOM) ATTN: AMSAT-R-NR, M/S 219-1 Ames Research Center Moffett Field, CA 94035-1000

No. of Copies	Organization
1	Commander U.S. Army Missile Command ATTN: AMSMI-RD-CS-R (DOC) Redstone Arsenal, AL 35898-5010
1	Commander U.S. Army Tank-Automotive Command ATTN: AMSTA-JSK (Armor Eng. Br.) Warren, MI 48397-5000
1	Director U.S. Army TRADOC Analysis Command ATTN: ATRC-WSR White Sands Missile Range, NM 88002-5502
(Class. only) 1	Commandant U.S. Army Infantry School ATTN: ATSH-CD (Security Mgr.) Fort Benning, GA 31905-5660
(Unclass. only) 1	Commandant U.S. Army Infantry School ATTN: ATSH-WCB-O Fort Benning, GA 31905-5000
1	WL/MNOI Eglin AFB, FL 32542-5000
	Aberdeen Proving Ground
2	Dir, USAMSAA ATTN: AMXSY-D AMXSY-MP, H. Cohen
1	Cdr, USATECOM ATTN: AMSTE-TC
1	Dir, ERDEC ATTN: SCBRD-RT
1	Cdr, CBDA ATTN: AMSCB-CII
1	Dir, USARL ATTN: AMSRL-SL-I
10	Dir, USARL ATTN: AMSRL-OP-CI-B (Tech Lib)

No. of Copies	Organization
1	Chairman DOD Explosives Safety Board Room 856-C Hoffman Bldg. 1 2461 Eisenhower Avenue Alexandria, VA 22331-0600
1	Headquarters U.S. Army Materiel Command ATTN: AMCICP-AD, M. Fisette 5001 Eisenhower Ave. Alexandria, VA 22333-0001
1	U.S. Army Ballistic Missile Defense Systems Command Advanced Technology Center P.O. Box 1500 Huntsville, AL 35807-3801
1	Department of the Army Office of the Product Manager 155mm Howitzer, M109A6, Paladin ATTN: SFAE-AR-HIP-IP, Mr. R. De Kleine Picatinny Arsenal, NJ 07806-5000
3	Project Manager Advanced Field Artillery System ATTN: SFAE-ASM-AF-E, LTC A. Ellis T. Kuriata J. Shields Picatinny Arsenal, NJ 07801-5000
1	Project Manager Advanced Field Artillery System ATTN: SFAE-ASM-AF-Q, W. Warren Picatinny Arsenal, NJ 07801-5000
2	Commander Production Base Modernization Agency U.S. Army Armament Research, Development, and Engineering Center ATTN: AMSMC-PBM, A. Siklosi AMSMC-PBM-E, L. Laibson Picatinny Arsenal, NJ 07806-5000
4	PEO-Armaments Project Manager Tank Main Armament System ATTN: AMCPM-TMA AMCPM-TMA-105 AMCPM-TMA-120 AMCPM-TMA-AS, H. Yuen Picatinny Arsenal, NJ 07806-5000
4	Commander U.S. Army Armament Research, Development, and Engineering Center ATTN: SMCAR-CCH-V, C. Mandala E. Fennell SMCAR-CCH-T, L. Rosendorf SMCAR-CCS Picatinny Arsenal, NJ 07806-5000
19	Commander U.S. Army Armament Research, Development, and Engineering Center ATTN: SMCAR-AEE, J. Lannon SMCAR-AEE-B, A. Beardell D. Downs S. Einstein S. Westley S. Bernstein J. Rutkowski B. Brodman P. O'Reilly R. Cirincione A. Grabowsky P. Hui J. O'Reilly SMCAR-AEE-WW, M. Mezger J. Pinto D. Wiegand P. Lu C. Hu SMCAR-AES, S. Kaplowitz Picatinny Arsenal, NJ 07806-5000
1	Commander U.S. Army Armament Research, Development and Engineering Center ATTN: SMCAR-HFM, E. Barrieres Picatinny Arsenal, NJ 07806-5000

No. of Copies	Organization
9	Commander U.S. Army Armament Research, Development and Engineering Center ATTN: SMCAR-FSA-F, LTC R. Riddle SMCAR-FSC, G. Ferdinand SMCAR-FS, T. Gora SMCAR-FS-DH, J. Feneck SMCAR-FSS-A, R. Kopmann B. Machek L. Pinder SMCAR-FSN-N, K. Chung Picatinny Arsenal, NJ 07806-5000
3	Director Benet Weapons Laboratories ATTN: SMCAR-CCB-RA, G.P. O'Hara G.A. Pflegl SMCAR-CCB-S, F. Heiser Watervliet, NY 12189-4050
2	Commander U.S. Army Research Office ATTN: Technical Library D. Mann P.O. Box 12211 Research Triangle Park, NC 27709-2211
1	Director Army Research Office ATTN: AMXRO-MCS, Mr. K. Clark P.O. Box 12211 Research Triangle Park, NC 27709-2211
1	Director Army Research Office ATTN: AMXRO-RT-IP, Library Services P.O. Box 12211 Research Triangle Park, NC 27709-2211
1	Commander, USACECOM R&D Technical Library ATTN: ASQNC-ELC-IS-L-R, Myer Center Fort Monmouth, NJ 07703-5301
1	Commandant U.S. Army Aviation School ATTN: Aviation Agency Fort Rucker, AL 36360

No. of Copies	Organization
1	Program Manager U.S. Tank-Automotive Command ATTN: AMCPM-ABMS, T. Dean Warren, MI 48092-2498
1	Project Manager U.S. Tank-Automotive Command Fighting Vehicle Systems ATTN: SFAE-ASM-BV Warren, MI 48397-5000
1	Project Manager, Abrams Tank System ATTN: SFAE-ASM-AB Warren, MI 48397-5000
1	Director HQ, TRAC RPD ATTN: ATCD-MA Fort Monroe, VA 23651-5143
1	Commander U.S. Army Belvoir Research and Development Center ATTN: STRBE-WC Fort Belvoir, VA 22060-5006
1	Director U.S. Army TRAC-Ft. Lee ATTN: ATRC-L, Mr. Cameron Fort Lee, VA 23801-6140
1	Commandant U.S. Army Command and General Staff College Fort Leavenworth, KS 66027
1	Commandant U.S. Army Special Warfare School ATTN: Rev and Trng Lit Div Fort Bragg, NC 28307
1	Commander Radford Army Ammunition Plant ATTN: SMCAR-QA/HI LIB Radford, VA 24141-0298

No. of Copies	Organization
1	Commander U.S. Army Foreign Science and Technology Center ATTN: AMXST-MC-3 220 Seventh Street, NE Charlottesville, VA 22901-5396
2	Commandant U.S. Army Field Artillery Center and School ATTN: ATSF-CO-MW, E. Dublisky ATSF-CN, P. Gross Ft. Sill, OK 73503-5600
1	Commandant U.S. Army Armor School ATTN: ATZK-CD-MS, M. Falkovitch Armor Agency Fort Knox, KY 40121-5215
2	Commander Naval Sea Systems Command ATTN: SEA 62R SEA 64 Washington, DC 20362-5101
1	Commander Naval Air Systems Command ATTN: AIR-954-Tech Library Washington, DC 20360
4	Commander Naval Research Laboratory ATTN: Technical Library Code 4410, K. Kailasanate J. Boris E. Oran Washington, DC 20375-5000
1	Office of Naval Research ATTN: Code 473, R.S. Miller 800 N. Quincy Street Arlington, VA 22217-9999

No. of Copies	Organization
1	Office of Naval Technology ATTN: ONT-213, D. Siegel 800 N. Quincy St. Arlington, VA 22217-5000
2	Commander Naval Surface Warfare Center ATTN: Code 730 Code R-13, R. Bernecker Silver Spring, MD 20903-5000
7	Commander Naval Surface Warfare Center ATTN: T.C. Smith K. Rice S. Mitchell S. Peters J. Consaga C. Gotzmer Technical Library Indian Head, MD 20640-5000
4	Commander Naval Surface Warfare Center ATTN: Code G30, Guns & Munitions Div Code G32, Guns Systems Div Code G33, T. Doran Code E23 Technical Library Dahlgren, VA 22448-5000
5	Commander Naval Air Warfare Center ATTN: Code 388, C.F. Price T. Boggs Code 3895, T. Parr R. Derr Information Science Division China Lake, CA 93555-6001
1	Commanding Officer Naval Underwater Systems Center ATTN: Code 5B331, Technical Library Newport, RI 02840
1	AFOSR/NA ATTN: J. Tishkoff Bolling AFB, D.C. 20332-6448

No. of Copies	Organization
1	OLAC PL/TSTL ATTN: D. Shiplett Edwards AFB, CA 93523-5000
3	AL/LSCF ATTN: J. Levine L. Quinn T. Edwards Edwards AFB, CA 93523-5000
1	WL/MNAA ATTN: B. Simpson Eglin AFB, FL 32542-5434
1	WL/MNME Energetic Materials Branch 2306 Perimeter Rd. STE 9 Eglin AFB, FL 32542-5910
1	WL/MNSH ATTN: R. Drabczuk Eglin AFB, FL 32542-5434
2	NASA Langley Research Center ATTN: M.S. 408, W. Scallion D. Witcofski Hampton, VA 23605
1	Central Intelligence Agency Office of the Central References Dissemination Branch Room GE-47, HQS Washington, DC 20502
1	Central Intelligence Agency ATTN: J. Backofen NHB, Room 5N01 Washington, DC 20505
1	SDIO/TNI ATTN: L.H. Caveny Pentagon Washington, DC 20301-7100
1	SDIO/DA ATTN: E. Gerry Pentagon Washington, DC 21301-7100

No. of Copies	Organization
2	HQ DNA ATTN: D. Lewis A. Fahey 6801 Telegraph Rd. Alexandria, VA 22310-3398
1	Director Sandia National Laboratories Energetic Materials & Fluid Mechanics Department, 1512 ATTN: M. Baer P.O. Box 5800 Albuquerque, NM 87185
1	Director Sandia National Laboratories Combustion Research Facility ATTN: R. Carling Livermore, CA 94551-0469
1	Director Sandia National Laboratories ATTN: 8741, G. A. Beneditti P.O. Box 969 Livermore, CA 94551-0969
2	Director Lawrence Livermore National Laboratory ATTN: L-355, A. Buckingham M. Finger P.O. Box 808 Livermore, CA 94550-0622
2	Director Los Alamos Scientific Lab ATTN: T3/D. Butler M. Division/B. Craig P.O. Box 1663 Los Alamos, NM 87544
2	Battelle ATTN: TACTEC Library, J.N. Huggins V. Levin 505 King Avenue Columbus, OH 43201-2693
1	Battelle PNL ATTN: M.C.C. Bampton P.O. Box 999 Richland, WA 99352

No. of Copies	Organization
1	Institute of Gas Technology ATTN: D. Gidaspow 3424 S. State Street Chicago, IL 60616-3896
1	Institute for Advanced Technology ATTN: T.M. Kiehne The University of Texas of Austin 4030-2 W. Braker Lane Austin, TX 78759-5329
2	CPIA - JHU ATTN: H. J. Hoffman T. Christian 10630 Little Patuxent Parkway Suite 202 Columbia, MD 21044-3200
1	Brigham Young University Department of Chemical Engineering ATTN: M. Beckstead Provo, UT 84601
1	Jet Propulsion Laboratory California Institute of Technology ATTN: L.D. Strand, MS 125/224 4800 Oak Grove Drive Pasadena, CA 91109
1	California Institute of Technology 204 Karman Lab Main Stop 301-46 ATTN: F.E.C. Culick 1201 E. California Street Pasadena, CA 91109
3	Georgia Institute of Technology School of Aerospace Engineering ATTN: B.T. Zim E. Price W.C. Strahle Atlanta, GA 30332
1	Massachusetts Institute of Technology Department of Mechanical Engineering ATTN: T. Toong 77 Massachusetts Avenue Cambridge, MA 02139-4307

No. of Copies	Organization
2	University of Illinois Department of Mechanical/Industry Engineering ATTN: H. Krier R. Beddini 144 MEB; 1206 N. Green St. Urbana, IL 61801-2978
1	University of Maryland ATTN: Dr. J.D. Anderson College Park, MD 20740
1	University of Massachusetts Department of Mechanical Engineering ATTN: K. Jakus Amherst, MA 01002-0014
1	University of Minnesota Department of Mechanical Engineering ATTN: E. Fletcher Minneapolis, MN 55414-3368
3	Pennsylvania State University Department of Mechanical Engineering ATTN: V. Yang K. Kuo C. Merkle University Park, PA 16802-7501
1	Rensselaer Polytechnic Institute Department of Mathematics Troy, NY 12181
1	Stevens Institute of Technology Davidson Laboratory ATTN: R. McAlevy III Castle Point Station Hoboken, NJ 07030-5907
1	Rutgers University Department of Mechanical and Aerospace Engineering ATTN: S. Temkin University Heights Campus New Brunswick, NJ 08903
1	University of Southern California Mechanical Engineering Department ATTN: OHE200, M. Gerstein Los Angeles, CA 90089-5199

No. of Copies	Organization
1	University of Utah Department of Chemical Engineering ATTN: A. Baer Salt Lake City, UT 84112-1194
1	Washington State University Department of Mechanical Engineering ATTN: C.T. Crowe Pullman, WA 99163-5201
1	AFELM, The Rand Corporation ATTN: Library D 1700 Main Street Santa Monica, CA 90401-3297
1	Arrow Technology Associates, Inc. ATTN: W. Hathaway P.O. Box 4218 South Burlington, VT 05401-0042
3	AAI Corporation ATTN: J. Hebert J. Frankle D. Cleveland P.O. Box 126 Hunt Valley, MD 21030-0126
2	Alliant Techsystems, Inc. ATTN: R.E. Tompkins J. Kennedy 7225 Northland Dr. Brooklyn Park, MN 55428
1	AVCO Everett Research Laboratory ATTN: D. Stickler 2385 Revere Beach Parkway Everett, MA 02149-5936
1	General Applied Sciences Lab ATTN: J. Erdos 77 Raynor Ave. Ronkonkama, NY 11779-6649
1	General Electric Company Tactical System Department ATTN: J. Mandzy 100 Plastics Ave. Pittsfield, MA 01201-3698
1	IITRI ATTN: M.J. Klein 10 W. 35th Street Chicago, IL 60616-3799

No. of Copies	Organization
4	Hercules, Inc. Radford Army Ammunition Plant ATTN: L. Gizzi D.A. Worrell W.J. Worrell C. Chandler Radford, VA 24141-0299
2	Hercules, Inc. Allegheny Ballistics Laboratory ATTN: William B. Walkup Thomas F. Farabaugh P.O. Box 210 Rocket Center, WV 26726
1	Hercules, Inc. Aerospace ATTN: R. Cartwright 100 Howard Blvd. Kenville, NJ 07847
1	Hercules, Inc. Hercules Plaza ATTN: B.M. Riggleman Wilmington, DE 19894
1	MBR Research Inc. ATTN: Dr. Moshe Ben-Reuven 601 Ewing St., Suite C-22 Princeton, NJ 08540
1	Olin Corporation Badger Army Ammunition Plant ATTN: F.E. Wolf Baraboo, WI 53913
3	Olin Ordnance ATTN: E.J. Kirschke A.F. Gonzalez D.W. Worthington P.O. Box 222 St. Marks, FL 32355-0222
1	Olin Ordnance ATTN: H.A. McElroy 10101 9th Street, North St. Petersburg, FL 33716
1	Paul Gough Associates, Inc. ATTN: P.S. Gough 1048 South St. Portsmouth, NH 03801-5423

No. of Copies	Organization
1	Physics International Library ATTN: H. Wayne Wampler P.O. Box 5010 San Leandro, CA 94577-0599
2	Princeton Combustion Research Laboratories, Inc. ATTN: N. Mer N.A. Messina Princeton Corporate Plaza 11 Deerpark Dr., Bldg IV, Suite 119 Monmouth Junction, NJ 08852
3	Rockwell International Rocketdyne Division ATTN: BA08, J. Flanagan J. Gray R.B. Edelman 6633 Canoga Avenue Canoga Park, CA 91303-2703
2	Rockwell International Science Center ATTN: Dr. S. Chakravarthy Dr. S. Palaniswamy 1049 Camino Dos Rios P.O. Box 1085 Thousand Oaks, CA 91360
1	Science Applications International Corp. ATTN: M. Palmer 2109 Air Park Rd. Albuquerque, NM 87106
1	Southwest Research Institute ATTN: J.P. Riegel 6220 Culebra Road P.O. Drawer 28510 San Antonio, TX 78228-0510
1	Sverdrup Technology, Inc. ATTN: Dr. John Deur 2001 Aerospace Parkway Brook Park, OH 44142
3	Thiokol Corporation Elkton Division ATTN: R. Willer R. Biddle Tech Library P.O. Box 241 Elkton, MD 21921-0241
1	Veritay Technology, Inc. ATTN: E. Fisher 4845 Millersport Hwy. East Amherst, NY 14501-0305
1	Universal Propulsion Company ATTN: H.J. McSpadden 25401 North Central Ave. Phoenix, AZ 85027-7837
1	SRI International Propulsion Sciences Division ATTN: Tech Library 333 Ravenwood Avenue Menlo Park, CA 94025-3493
	Aberdeen Proving Ground
1	Cdr, USACSTA ATTN: STECS-PO/R. Hendricksen

USER EVALUATION SHEET/CHANGE OF ADDRESS

This Laboratory undertakes a continuing effort to improve the quality of the reports it publishes. Your comments/answers to the items/questions below will aid us in our efforts.

1. ARL Report Number ARL-TR-198 Date of Report September 1993

2. Date Report Received _____

3. Does this report satisfy a need? (Comment on purpose, related project, or other area of interest for which the report will be used.) _____

4. Specifically, how is the report being used? (Information source, design data, procedure, source of ideas, etc.) _____

5. Has the information in this report led to any quantitative savings as far as man-hours or dollars saved, operating costs avoided, or efficiencies achieved, etc? If so, please elaborate. _____

6. General Comments. What do you think should be changed to improve future reports? (Indicate changes to organization, technical content, format, etc.) _____

CURRENT ADDRESS

_____
Organization

_____
Name

_____
Street or P.O. Box No.

_____
City, State, Zip Code

7. If indicating a Change of Address or Address Correction, please provide the Current or Correct address above and the Old or Incorrect address below.

OLD ADDRESS

_____
Organization

_____
Name

_____
Street or P.O. Box No.

_____
City, State, Zip Code

(Remove this sheet, fold as indicated, tape closed, and mail.)
(DO NOT STAPLE)

DEPARTMENT OF THE ARMY

OFFICIAL BUSINESS

BUSINESS REPLY MAIL
FIRST CLASS PERMIT No 0001, APG, MD

Postage will be paid by addressee

Director
U.S. Army Research Laboratory
ATTN: AMSRL-OP-CI-B (Tech Lib)
Aberdeen Proving Ground, MD 21005-5066

NO POSTAGE
NECESSARY
IF MAILED
IN THE
UNITED STATES